Spectral signatures of Earth's climate variability over 5 years from IASI

Helen Brindley, Richard Bantges, Jacqueline Russell, Jonathan Murray, Christopher Dancel, Claudio Belotti and John Harries

Space and Atmospheric Physics Group, Imperial College, London

This is the peer reviewed version of the following article: Brindley, H, R. Bantges, J. Russell, J. Murray, C. Dancel, C. Belotti and J. Harries (2015), Spectral signatures of Earth's climate variability over 5 years from IASI, J. Climate, 28, 1649-1660, which has been published in final form at http://dx.doi.org/10.1175/JCL-D-14-00431.1.

Corresponding author address: Helen Brindley, Space and Atmospheric Physics Group, Imperial College London, Blackett Laboratory, Prince Consort Road, London, SW7 2AZ, UK

E-mail: h.brindley@imperial.ac.uk

Abstract

Interannual variability in spectrally resolved longwave radiances is quantified at a variety of spatial scales using five years of IASI observations. Maximum variability is seen at the smallest scales investigated (10° zonal means) at northern and southern high latitudes across the centre of the 15 μm CO_2 band. As spatial scale increases, the overall magnitude of interannual variability reduces across the spectrum and the spectral shape of the variability changes. In spectral regions sensitive to conditions in the upper troposphere the effect of increasing spatial scale is relatively small and at the global scale these parts of the spectrum show the greatest year-to-year variability. Conversely the atmospheric window (8-12 μm), which is sensitive to variations in surface temperature and cloud, shows a marked reduction in interannual variability with increasing spatial scale. Over the five years studied, at global scales the standard deviation in annual mean brightness temperature is less than 0.17 K across the spectrum; reducing to less than 0.05 K across the window. Spectrally integrating the IASI measurements to create pseudo broadband and window channels indicates a variation about the mean that is higher for the broadband than the window channel at the global and quasi-global scale and over the southern hemisphere. These findings are in agreement with observations from CERES *Terra* over the same period and imply that at the largest spatial scales, over the period considered here, fluctuations in mid-upper tropospheric temperatures and water vapour, and not cloud or surface temperature, play the dominant role in determining the level of interannual variability in all-sky outgoing longwave radiation.

1. Introduction

The potential for using measurements of spectrally resolved outgoing longwave radiation (OLR) directly to monitor the climatic state and detect and attribute change has been recognised for some time (e.g. Charlock *et al*., 1984, Kiehl *et al*., 1986, Goody *et al*., 1995, Iacono and Clough, 1996, Slingo and Webb, 1997, Harries *et al*., 2001). More recently interest in the topic has revived due to the prospect of a dedicated space mission, CLARREO (Climate Absolute Radiance and Refractivity Observatory), which seeks to establish high absolute accuracy benchmark climate observations of spectrally resolved thermal infrared and reflected solar radiation, in combination with measurements of atmospheric refraction (Wielicki *et al*., 2013). Theoretical studies by members of the CLARREO science team have shown how distinct longwave spectral signals from different climate forcing and feedback mechanisms may be derived, and, importantly in the context of the temporal and spatial sampling strategy envisaged for CLARREO, appear to combine with a high degree of linearity (Leroy *et al*., 2008, Huang *et al*., 2010).

To date, attempts to evaluate changes in the forcing of climate and associated feedback processes by considering changes over time to spectrally resolved OLR observations of the Earth have typically been restricted to clear-sky conditions (Harries *et al*., 2001, Griggs and Harries, 2007). These studies demonstrated that sharp spectral features due to long-term increases in concentration of individual molecules such as CO_2, CH_4 and CFCs can be identified. However, the detection of changes in the outgoing spectrum that might be due to water vapour and, in particular, cloud feedback processes are much more difficult to unambiguously discern (e.g. Brindley and Allan, 2003). In particular, the high level of variability in the cloud field in space and time not only has implications for the interpretation of spatially and temporally averaged radiances (e.g. Kato *et al*., 2011), but crucially, makes disentangling responses to climate forcing from underlying climate variability a hugely challenging task. Whilst there have been several studies on the impact that temporal and spatial sampling may have on the accuracy with which climate change signals can be detected in OLR observations (Brindley and Harries, 2003a; Brindley and Harries, 2003b, Kirk-Davidoff *et al*., 2005), understanding the exact nature and level of background variability seen in observed all-sky spectra is an important question which has not yet been fully addressed.

Recognising this challenge, the work presented here exploits the emerging radiance record available from the Infrared Atmospheric Sounding Interferometer (IASI) on the European Metop satellite (Hilton *et al*., 2012) to investigate the interannual variability in average OLR spectra at different spatial scales. Results are placed in the context of broadband observations from the Clouds and the Earth's Radiant Energy System (CERES) instruments (Wielicki *et al*., 1996) to assess both the consistency between the different records and the additional insights that can be gained from the higher spectral resolution available from IASI. Hence, in section 2 we briefly introduce IASI and CERES before focusing on the insights provided by the former instrument in section 3. Where appropriate we also make reference to the results presented in Huang and Ramaswamy (2009) who, in their efforts to assess the time evolution of spectral OLR, evaluated the monthly and annual variability seen in global mean observations from the Atmospheric InfraRed Sounder (AIRS) (Chahine *et al*., 2006) over the period 2002-2007. We show that the interannual variability manifested across the IASI spectra is less than 0.17 K in brightness temperature in the global annual mean, collapsing to a value of less than 0.05 K in the so-called atmospheric window (~800-1250 cm^{-1}), a remarkable result with implications for the variability of the cloud field and the land surface. In section 4 we use the observations from CERES to illustrate that these results are consistent with patterns of behaviour seen in both broadband and window OLR fluxes and investigate issues related to instrument sampling. We discuss the potential implications of these results, as well as the caveats associated with our study in section 5.

2. Observational Tools

a. IASI

IASI is a Michelson Interferometer, covering the spectral range from 645 to 2760 cm^{-1} in three separate wavenumber bands running from 645-1210, 1210-2000 and 2000-2760 cm^{-1} (Simeoni *et al.*, 2004) with an apodised half-width of 0.5 cm^{-1}. Since October 2006 it has enabled high-resolution atmospheric sounding from the sun-synchronous Metop-A platform which has an equator crossing time of 0930 local time for the descending node. The instrument is a cross-track scanner, producing 30 'fields of regard' (FOR) per scan; each is an array of 2 x 2 pixels with a 12 km diameter at nadir. Instrument noise levels are found to be within specification and stable over time except for wavenumbers below 680 cm^{-1} and in small band overlap regions where observations from different detectors are merged (Blumstein *et al.*, 2007). In the spectral region of interest for this study NEΔT levels (expressed at 280K) are always below 0.4 K (minimum wavenumber ~ 660 cm^{-1}) and more typically less than 0.3 K. Comparisons with co-located observations from the Atmospheric InfraRed Sounder indicate agreement between the two instruments to within +/-0.2K, while calibration/validation activities using aircraft based interferometers give agreement to within +/-0.3 K (Newman *et al.*, 2008, Larar *et al.*, 2010).

Here we use only 'nadir' IASI observations (in practice, within 5° of nadir) covering the spectral range 645-1600 cm^{-1} which, over the five years from January 2008 to December 2012, yields

~160 million spectra as input to the study. As neither high spatial nor spectral resolution is a priority, initial data reduction to the ~100 km spatial scale is made by averaging 16 IASI near nadir spectra and the result smoothed to a 2.8 cm^{-1} spectral resolution, with a view to facilitating comparisons with previous analyses which used data from the IRIS mission (Hanel *et al*., 1972) in future studies. The resulting IASI reduced resolution (hereafter IRR) spectra form the basic input to the averaging studies discussed in the following section and are comparable in spectral and spatial detail to those used in the work of Harries *et al*. (2001) and Griggs and Harries (2007). Figure 1 illustrates the global, annual mean IRR spectrum for 2008-2012 to place the variability plots shown in later sections in context. Principal spectral features are due to CO_2 (~650-800 cm^{-1}), O_3 (~1000-1070 cm^{-1}), CH_4 (~1200-1400 cm^{-1}, centred at 1303 cm^{-1}), and H_2O (~1250-1600 cm^{-1}), with other weaker bands also in evidence, e.g. $CFCl_3$ (853 cm^{-1}).

In the large scale annual averages presented in this study at least 1.6 million native resolution IASI spectra are used to obtain the final IRR results. If the source of the 0.4 K NEΔT error indicated above was purely random in nature this would translate to a final uncertainty that is of the order 3 x 10^{-4} K in zonal mean averages, and a factor of ~4 smaller in the global mean. In reality it is likely that there is a systematic component to the NEΔT that is not reduced by averaging and cannot be estimated easily. However, since we are focussed on diagnosing variability in this study, it is the stability of IASI which is paramount. Comparisons with AIRS show radiometric agreement between the two instruments that is within a few mK or better (Hilton *et al*., 2012 and references therein) suggesting excellent stability over time.

b. CERES

Since 2001 CERES has provided global measurements of the Earth's Radiation Budget from low earth orbit (Wielicki *et al*., 1996). Besides contributing to numerous important studies of the effects of different climate processes on the Earth's energy balance, the uncertainties associated with the measurements have also been rigorously assessed and documented (e.g. Loeb *et al*., 2009). In this study we make use of observations from the *Terra* and *Aqua* platforms over the same 2008-2012 period considered for IASI. The CERES instrument measures the broadband shortwave radiation reflected at the top of the atmosphere (TOA) in conjunction with the total outgoing longwave radiation (OLR), the latter nominally covering the range 5-100 μm. In addition, observations are also made in a longwave window channel sensitive to radiation between approximately 8-12 μm. In order to make use of these window fluxes we employ level 3 monthly mean files provided at 1° latitude-longitude resolution, derived from single-scanner footprints (so called SSF1deg_Ed2.7). Note that these products are created from hourly data which are obtained using temporal interpolation assuming constant meteorology. Over non snow covered land, during the day a half-sine fit is used, with night-time fluxes set to a constant value if the daytime flux is greater than the night-time value. Over ocean and snow, linear interpolation is used between the CERES overpass times.

3. Inter-annual variability in IRR spectra

a. 10° Zonal Means

We begin by considering the interannual variation in IRR brightness temperature spectra at the 10° zonal scale, as this spatial scale is consistent with the type of averages expected to be produced by the CLARREO mission. Figure 2 shows the standard deviation across the 5 years in the annual-mean brightness temperatures, σ_{TB}, for 10° zonal bands in the northern (a) and southern (b) hemisphere. Maximum σ_{TB}s occur across the 15 μm CO_2 band centre (from ν~ 645-700 cm^{-1}) at northern and southern high latitudes, peaking at ~ 690 cm^{-1} in these zones. Noting the noise characteristics of IASI we focus our discussions on observations in excess of 660 cm^{-1}. Emission to space at the very centre of the band at 667 cm^{-1} originates from the mid-upper stratosphere. Moving away from the central peak, emission to space occurs from systematically lower levels in the stratosphere, until by ~ 680 cm^{-1} one is effectively sounding the tropopause. As wavenumber increases over the CO_2 band wing (~700-760 cm^{-1}), emission from successively lower levels in the troposphere is observed (see Fig. 1).

Distinct peaks in σ_{TB} are also seen in the centre of the 1303 cm^{-1} CH_4 band and strong water vapour lines at wavenumbers > 1500 cm^{-1}. These are largest within the 80-90° zones but are still clearly apparent at lower latitudes, particularly in the southern hemisphere. Within the northern hemisphere, variability within the atmospheric window region (ν ~ 800-1250 cm^{-1}) is typically higher than that seen within the CO_2 band wing (from 720-760 cm^{-1}) and across the 6.3 μm water vapour vibration-rotation band (ν > 1250 cm^{-1}). No consistent pattern with latitude is seen within the 9.6 μm O_3 band (ν ~1000-1070 cm^{-1}), although for the majority of zones the variability here is higher than across the atmospheric window as a whole. We note that the window region would be expected to be particularly sensitive to variations in surface temperature and cloud, with the changes in spectral shape we see here potentially reflecting variability in cloud microphysical properties (e.g. Strabala *et al*., 1994). In this study we make no attempt to separate out the different factors controlling this variability but anticipate that this will be an area for future investigation.

b. 30° Zonal Means

Moving to larger scales, Figure 3 shows the interannual standard deviation in brightness temperature for 30° zones across both hemispheres. Here 30° zonal mean radiances are constructed from the 10° zonal mean radiances employed in section 3(a), applying equal weighting to each band, before converting to brightness temperature and calculating the associated standard deviation. The first point to note is that, as might be expected (e.g. Brindley and Harries, 2003a,b; Kirk-Davidoff *et al*., 2005), the overall level of σ_{TB} is decreased, falling to a maximum level of 0.9 K (compared to 1.15 K) across the CO_2 band centre at southern hemisphere high latitudes (Fig. 3(b)). For both hemispheres the 60-90° band shows the largest σ_{TB} within the window region. While these values reduce rather dramatically in the southern hemisphere within the lower latitude bands, the reduction in the northern hemisphere is much less marked. Excepting the 9.6 μm O_3 band, within the 0-30°S and 30-60°S bands variability across the window is lower than other spectral regions (such as within the water vapour vibration-rotation band and 15 μm CO_2 band wing), behaviour that is not exhibited in any of the other latitude bands.

Outside of the window the behaviour within the highest latitude zones is most striking. Consistent with the higher spatial resolution results, maximum σ_{TB}s occur across the 15 μm CO_2 band centre and at the peak of the 1303 cm^{-1} CH_4 band, particularly in the southern hemisphere. The signatures of increased variability due to the strong water vapour lines at wavenumbers greater than 1500 cm^{-1} are also still apparent within these zones.

c. Global Mean

Focusing now on the largest spatial scale, Figure 4(a) shows the differences from the mean spectrum shown in Fig. 1 for each year from 2008-2012. Immediately apparent is the degree of stability over the five years sampled here, with year-to-year differences of less than 0.3 K across the spectral region covered (equivalent to radiance differences of < 0.3 mW m^{-2} sr^{-1}). This level of stability translates to the standard deviations in spectrally resolved global annual mean brightness temperature shown in Figure 4(b). Similar to section 3(b), annual global mean radiance spectra were constructed from the 10° zonal means of section 3(a), applying the appropriate area (cosine) weighting to each band, prior to conversion to brightness temperature and calculation of standard deviation.

Across the entire spectral region the interannual global σ_{TB}s are very small, at less than 0.17 K. While the reduction in overall variability with increasing spatial scale might be anticipated, the impact of global averaging alters with spectral region, resulting in a distinct change in spectral shape. Figure 4(b) indicates that at the global scale, rather than peaking in the 15 μm CO_2 band centre, variability peaks within the CO_2 band wing (700-740cm^{-1}) and at the centre of the 1303 cm^{-1} CH_4 band. Note that because of the non-linearity of the transformation from radiance to brightness temperature the impact of the variation on outgoing energy is larger in the former spectral region. Enhanced variability is also seen beyond 1350cm^{-1} within the 6.3 μm H_2O vibration-rotation band with a further, secondary peak in σ_{TB} apparent across the 9.6 μm O_3 band. Surprisingly, perhaps, in the context of Figures 2 and 3, the lowest level of variability is seen within the atmospheric window (excluding the O_3 band) at less than 0.05 K.

Returning to Fig 4(a) it is interesting to note that removing one year (2010) from the analysis can markedly affect the magnitude of the interannual variability in some spectral regions and hence the spectral shape. The early months of 2010 were associated with a strong El Niño (large positive multivariate El Niño Southern Oscillation index (MEI) values) before transitioning to an even stronger La Niña in the summer. During El Niño conditions one typically sees positive anomalies in OLR even at the global scale, with the converse being true for a La Niña phase (e.g. Loeb *et al*., 2012, Susskind *et al*., 2012). The positive brightness temperature differences seen during 2010 across the majority of the spectrum would suggest that enhanced planetary emission has in some sense 'won' over the course of the year. What is particularly noteworthy is the peak seen across the 1303 cm^{-1} CH_4 band and the somewhat enhanced positive difference in the CO_2 band wing. Both are indicative of anomalously warm mid-upper tropospheric temperatures. With 2010 removed, anomalies from the 4 year (2008, 2009, 2011, 2012) mean are significantly reduced (< 0.15 K), with a peak associated standard deviation of less than 0.1 K (Fig 4(b)). In this case, although the window region still shows minimum variation, the peak brightness temperature variability is no longer seen at 1303 cm^{-1}, but rather across the 6.3 μm H_2O vibration-rotation band at wavenumbers > 1400 cm^{-1}, within the 9.6 μm O_3 band, and both within the 15 μm CO_2 band wing and at the very centre of the band. While the full 2008-2012 period considered here does sample a relatively wide range of MEI values, these results indicate how the magnitude and spectral shape of estimates of variability are themselves critically dependent on the period sampled, particularly with respect to major global and regional events such as El Niño.

With this in mind it is informative to compare Figure 4(b) to the results shown in Figure 3(a) of Huang and Ramaswamy (2009) who carried out a similar analysis using AIRS observations from

2002-2007. In their work the magnitude of global annual mean variability across the same spectral region as considered here does not exceed 0.16 K, but peaks in the centre of the 15 μm CO_2 band. While a secondary peak is seen in the CO_2 band wing, the relative variability seen across the window and the 1250-1500 cm^{-1} wavenumber range is of a different sense to that seen here, with larger variability in the former region compared to the latter. In addition, the variability across the window manifested in the AIRS measurements is also slightly larger than that seen here, reaching ~0.07 K. Results for smaller spatial scales are not presented by Huang and Ramaswamy but it is interesting to note that for the majority of the period they considered the climate system was in an El Niño phase. Moreover, the range in MEI values was smaller than that seen over the 2008-2012 period.

4. Comparison to broadband observations

a. Window, non-window and broadband variability as a function of spatial scale

In this section we seek to investigate whether the spectrally resolved results seen in section 3 are consistent with spectrally integrated observations made over the same 5 year period. To this end we employ CERES *Terra* and *Aqua* broadband OLR and window fluxes. CERES window fluxes cover the range ~833-1250 cm^{-1} so by comparing them to the corresponding OLR measurements we can assess whether a reduction in window relative to non-window interannual variability is seen as spatial scale increases, as might be anticipated from the IRR results. In addition, by spectrally integrating the IRR data over the appropriate wavenumber range we can perform a direct comparison with IRR window radiances. For completeness, a similar integration has also been performed over the full 660-1600 cm^{-1} range studied here to create 'broadband' IRR radiances. However, these do not sample the energetically important far infra-red region (Sinha and Harries, 1995; Harries *et al*., 2008), the majority of which is captured by the CERES OLR fluxes. Because of the different metrics being compared, the variability is presented in terms of coefficient of variation (CV) which is simply the inter-annual standard deviation, σ, divided by the five year annual mean for each dataset, μ, expressed as a percentage (Eq. (1)).

$$CV = 100 \times \frac{\sigma}{\mu} \tag{1}$$

In addition, it should be noted that:

$$\mu_{BB} = \mu_{win} + \mu_{nw} \quad \text{and} \quad \sigma_{BB} = \sqrt{\sigma_{win}^2 + \sigma_{nw}^2 + 2\,\mathrm{cov}(win, nw)} \tag{2}$$

where BB, win and nw subscripts refer to the broadband, window and non-window region respectively, and cov(win,nw) is the covariance between the window and non-window regions.

Figure 5(a) shows the interannual variability in CERES *Terra* and *Aqua* window channel fluxes as a function of latitude. Superimposed is the equivalent CV in IRR window radiances. It is clear that all three instruments show a very similar pattern of behaviour, with minimum window variability in the southern hemisphere low and mid-latitudes. It is also clear that the variability about the mean for all three datasets is very low, typically less than 1 %. Peak variability is seen in the 70-90° latitude bands with, in the southern hemisphere, larger variability being manifested in the CERES measurements. In the northern high latitudes the pattern switches such that IRR variability is typically higher. For a given latitude band, the difference between the CVs calculated for each instrument is generally less than 0.05 %. However, three bands display noticeably higher discrepancies between the instruments: 70-80°S and 0-10°N where the IRR CV is lower than that of the two CERES instruments, and 80-90°N where the opposite is true.

Detailed analysis of these bands has not identified any obviously anomalous behaviour for the two CERES instruments or for IASI and it should be noted that the latitudinal pattern is still consistent between the three instruments. Figure 5(a) thus gives confidence that, despite the differing overpass times and instrument characteristics of CERES *Terra*, *Aqua* and IASI, the general pattern and level of interannual variability exhibited in window fluxes and radiances sampled by the three instruments over the five years considered here is similar. Figure 5(b) shows how the relative level of variability in the different spectral ranges changes with scale. In section 3 the analysis of IRR spectra showed that as one moved from smaller to larger spatial scales the variation in the window region typically reduced more rapidly than in spectral regions outside of the window. Figure 5(b) confirms that this behaviour is also captured in the spectrally integrated IRR data and for the two CERES instruments. Whilst variability always reduces as the scale increases, at the 10 and 30° scale for all three instruments the mean window CV exceeds the equivalent non-window and broadband CVs by some margin. However, globally the non-window CV is similar in value or exceeds both the window and broadband CVs. This greater reduction in the window variability with spatial scale indicates that non-window variability becomes increasingly important and is most significant for the global average.

Furthermore, the influence of variability in spectral regions not sampled by the IRR broadband radiances (ν < 660 cm^{-1}, ν > 1600 cm^{-1}) is more significant at the global scale. Recall that the CV is the interannual standard deviation divided by the five year annual mean. At the 10 and 30° scales the larger spectral range of the CERES compared to the IRR broadband must lead to a greater increase in the mean for CERES when moving from window to broadband channel. The results show that this increase is not compensated sufficiently by the additional variability found at wavenumbers below 660 and above 1600 cm^{-1}. Thus the broadband CERES CVs are systematically smaller than the IRR cases. However for the global average the broadband CVs are similar for all three instruments indicating that at this scale the variability in the spectral regions not sampled by the IRR broadband is sufficient to compensate for their additive effect on the mean. This hints at an important role for the far infra-red region of the spectrum in determining all-sky OLR variability at the global scale.

b. Role of land/ocean sampling

In this section we provide an indication of the potential impact of spacecraft sampling patterns on the relative level of inter-annual variability seen between the window and broadband OLR. CERES *Terra* and *Aqua* are in sun-synchronous orbits with nominal ascending/descending local equator crossing times of 10.30/22.30 and 13.30/01.30 respectively. IASI is also in a sun-synchronous orbit, with a nominal local equator crossing time of 09.30 (21.30). While the annual means created from IASI are representative purely of the conditions at the observation time, as noted in section 2.2, the CERES means will contain the effects of temporal interpolation assuming constant meteorology between the instrument overpasses. We note however that using the Geostationary Enhanced 'SYN1deg' CERES products does not markedly affect the results reported here, suggesting that a more explicit representation of the diurnal cycle, using the observations made by the individual CERES instruments as anchor points, does not influence OLR variability at the spatial and temporal scales considered here.

The ability of a sun-synchronous orbit to truly capture the annual mean brightness temperature and its variability from year to year will depend on its overpass time due to a susceptibility to the phase of the diurnal cycle. Effects of this type are discussed in detail by Kirk-Davidoff *et al*. (2005) in the context of smaller, 15 by 30° grid box averages. They use 3 hourly 11 μm brightness temperatures, BT11, from the Global Cloud Imagery project (Salby *et al.*, 1991) to assess the effects of different sampling strategies on the associated sampling error. Most pertinently in the context of this study, they show that, although a sun-synchronous orbit will never represent the optimal solution for capturing the true diurnal behaviour, a 10 am/pm equator crossing time would be expected to minimise the error seen from this type of orbit and that the year to year bias errors are highly correlated. Nonetheless, they note that interannual variability in the diurnal cycle will introduce an additional component of variability into estimates of the mean made from sun-synchronous data. We might expect that these effects would be largest in locations where the magnitude of the diurnal cycle is largest. In addition, they should be manifested in spectral regions that are most sensitive to these variations.

Figure 6(a) shows the relative magnitude of window and broadband CV for each instrument for a variety of spatial regions of intermediate scale. In the northern hemisphere, tropics and deep tropics, the ratio of window to broadband CV is very similar for the two CERES instruments and systematically smaller for IASI. This difference is consistent with the results presented in Figure 5(b) and the associated discussion. However, over the southern hemisphere there is a marked discrepancy between *Terra* and *Aqua*, with the former showing a much reduced ratio relative to the latter. The equivalent IASI ratio is intermediate between the two values. Investigation of the contributing factors indicates that it is the window channel standard deviation which is responsible for this behaviour, being approximately halved for *Terra* relative to *Aqua* when considering the southern hemisphere as a whole. Given the land-ocean distribution we might expect any sensitivity to interannual variability in the diurnal cycle (and hence overpass time) to be more marked in the northern hemisphere so this result is rather surprising. What is more consistent with expectation is the reduction in window standard deviation seen between the northern and southern hemisphere for all instruments, which is reflected in the lower CV ratios over the southern hemisphere.

This reduction in window to broadband CV ratio over the southern hemisphere, coupled with the very low window standard deviations seen in oceanic bands (e.g. Fig. 2(b): 50-60°S) does indicate that instrument sampling will influence the exact magnitude and spectral distribution of variability, even at the extended temporal and spatial scales considered here. Figure 6(b) is an attempt to illustrate this more clearly using the IRR observations. Here the data have been sub-divided into land, ocean, day and night sub-categories prior to averaging. For all regions the window relative to the broadband CV is enhanced when only land scenes are considered. The most spectacular ocean/land differences are seen for the northern hemisphere case, where a negative covariance between the window and non window parts of the spectrum results in very low broadband standard deviations over land. More typically, the window and broadband standard deviations over land are both enhanced relative to those seen over ocean but the fractional increase relative to the mean is larger for the window channel. Restricting each region to ocean scenes only, the window CV is always comparable to, or smaller than, the equivalent broadband value.

5. Discussion and Conclusions

In this study we have used five years of IASI observations to assess the level of inter-annual variability seen within the Earth's outgoing longwave radiation spectrum (from 660-1600 cm^{-1}) at a variety of spatial scales ranging from 10° zonal means to global averages. Our results indicate that on these timescales, peak interannual variability at the smallest spatial scales is seen across the centre of the 15 μm CO_2 band (660-690 cm^{-1}) at high latitudes. At the very centre of the band (~667 cm^{-1}) this is likely a reflection of variation in planetary wave activity and, particularly in the northern hemisphere, the effects of sudden stratospheric warmings (e.g. Charlton and Polvani, 2007). The variability at wavenumbers between ~670-690 cm^{-1}, sounding the tropopause, is consistent with the fact that the seasonal cycle in tropopause temperature peaks over southern hemisphere high latitudes with a secondary maximum over the Arctic, and can show significant inter-annual variability over both locations (e.g. Kishore *et al*., 2006).

As spatial scale increases the interannual variability reduces across the spectrum, but this reduction occurs at a different rate for different spectral regions. While the interannual variability within the atmospheric window, most sensitive to surface temperature and cloud, reduces relatively rapidly with scale, variability in areas of the spectrum sensitive to mid-upper troposphere temperature and water vapour shows a slower reduction. As a consequence, at the global scale, interannual variability peaks in the wing of the 15 μm CO_2 band, across the 1303 cm^{-1} CH_4 band, and within the 6.3 μm water vapour vibration-rotation band at wavenumbers greater than 1400 cm^{-1}. At this global scale, interannual variability across the entire spectrum is less than 0.17 K, reducing to less than 0.05 K across the window. These values translate to equivalent radiance values of 0.17 and 0.05 mW m^{-2} cm sr^{-1} and highlight the remarkable stability of longwave emission from our planet as a whole. Similar findings in terms of the magnitude of spectral variability were reported by Huang and Ramaswamy (2009) based on analysis of AIRS data from 2002-2007. However, in that work the spectral shape of the variability was different to what we obtain here from IASI. It is an open question as to whether this change in shape is a result of the different periods covered, the different overpass times of the satellites carrying AIRS and IASI, or a result of instrument performance. Nonetheless, results of this type put observationally based limits on how the Earth's spectral emission to space varies interannually on the global scale, an important constraint which can be used to test and improve climate models.

Using broadband and window fluxes from the CERES instruments on *Terra* and *Aqua* we have shown that as spatial scale increases the OLR displays a similar reduction in inter-annual variability and is consistent with the spectral analysis in how this scaling behaviour differs in different spectral regions. At the smallest scales, the percentage variation about the mean (the coefficient of variation, CV) is substantially larger for the window channel compared to the broadband. As scale increases the CV in each spectral regime becomes more equivalent until at the global scale, for CERES *Terra* at least, the broadband CV exceeds that seen in the window channel. This behaviour arises because of the increasing importance of the variation from spectral regions outside of the window to the total broadband variance. Equivalent behaviour is seen in suitably spectrally integrated IASI observations.

Previous work has illustrated a strong anti-correlation between cloud and surface temperature variations within the tropics which may result in a compensation effect across the atmospheric window at the global scale (e.g. Huang and Ramaswamy, 2008). While OLR across the remainder of the longwave spectrum would also be affected by the presence of cloud, the impact of low and mid-level cloud across much of the spectrum is strongly damped by overlying upper tropospheric water vapour. It is feasible that high level cloud and surface temperature variations compensate each other in such a way that there is a minimal signal across the window coupled with enhanced variability in the CO_2 band wing and water-vapour vibration-rotation band. However, we have performed a set of realistic spectral simulations (to be reported in a follow on study) that do not show this behaviour. It also appears inconsistent with the findings of Huang and Ramaswamy (2009). There, much larger changes are seen across the window than within the water vapour bands or CO_2 band wing when comparing all-sky to clear-sky conditions. Hence, at the global and quasi-global scale we argue that our results imply that it is fluctuations in mid-upper tropospheric temperatures and water vapour, and not cloud or surface temperature, that play the dominant role in determining the level of inter-annual all-sky OLR variability, at least over the period we have considered here.

Given current interest in developing climate monitoring missions that will explicitly use spectrally resolved information it is interesting to note the potential effects of sampling and record length on the robustness of our findings. A reliable estimate of background variability is a key tool for determining whether a particular spectral signal is indicative of a true change or simply a climate fluctuation, and to identify which spectral regions offer the most promise for rapid change detection (e.g. Goody *et al.*, 1995). Hence, factors that can perturb both the magnitude and spectral shape of the background variability need to be understood and their effects quantified.

Decomposing the IASI results further has allowed us to provisionally probe the effects of sampling on our results. Splitting the data into land and ocean, and day and night categories indicates that enhanced variability is seen over land scenes, manifested through the magnitude of, in particular, window channel interannual standard deviations. This effect means that, even at the global scale, IASI window radiances show a larger CV than their broadband counterparts when only land scenes are averaged. Conversely, when only ocean scenes are included in the spatial averaging the window CV falls below that seen for the broadband for a number of regions including the deep-tropics, tropics and both hemispheres. These findings suggest that the precise satellite overpass time will affect both the magnitude and shape of any temporally and spatially averaged spectra that are produced. Similar conclusions can be drawn regarding the effects of record length on the variability exhibited within that record. While these results indicate the care that must be attached to interpreting the results from a given satellite record, previous work suggests that for instruments in sun-synchronous orbit, an early morning equator crossing time, similar to that of both IASI and CERES *Terra* will minimise diurnal sampling errors (Kirk-Davidoff *et al*., 2005). When all scenes are included in this study a smaller CV for the window compared to broadband is seen for IASI for the southern hemisphere, quasi-global and global mean cases, and this pattern of behaviour is replicated by CERES *Terra*. Similarly even when individual years are excluded from the period of study, minimum variability at the global scale is still seen across the atmospheric window.

It should be noted that in the analysis presented here there is no attempt to account for any trends, either real, or arising as a result of instrument performance, in the IRR data. There have certainly been real, monotonic increases in the annual mean concentrations of certain greenhouse gases (e.g. CO_2, CH_4) over the 2008-2012 time period and these would be expected to enhance absorption in those regions of the OLR spectrum sensitive to their presence. Acting in isolation this increased absorption would drive the OLR in a consistent direction with time, however, in reality any response will be modified by the temperature variability over the vertical levels where the absorption is taking place. Figure 4(a) suggests that no consistent linear trend in spectral OLR as measured by IASI exists with time across the wavenumber range considered here, at least at the global, annual mean scale. Turning to instrumental effects, while the absolute accuracy of the measurements cannot be quantified, studies have shown that the radiometric performances of IASI and AIRS agree to within a few mK or less as a function of time (Hilton *et al*., 2012) implying excellent temporal stability.

There is clearly a substantial amount of further information that can be extracted from the IASI data. In the short-term work is ongoing to establish whether the variability highlighted here is replicated in atmospheric reanalysis datasets and, if so, what processes drive this behaviour. Plans are in place to perform a detailed comparison with measurements from the AIRS instrument spanning the same time period, and the IASI data will also allow a re-evaluation of previous analyses comparing spectra measured in 1970 by the IRIS instrument on Nimbus-4 (Hanel *et al*., 1972) to assess whether it is possible to unambiguously identify 40 year plus change signals in all-sky data from the two instruments.

Acknowledgements

CERES data were extracted from http://ceres.larc.nasa.gov/order_data.php. IASI L1c data were obtained from the NERC Earth Observation Data Centre (NEODC). RJB, CD and CB were supported by the National Centre for Earth Observation (NCEO).

References

Blumstein, D., B. Tournier, F. Cayla, T. Phulpin, R. Fjortoft, C. Buil and G. Ponce, 2007, In-flight performance of the infrared atmospheric sounding interferometer (IASI) on METOP-A. Proceedings of SPIE, 6684, H6840-H6840

Brindley, H. and R. Allan, 2003, Simulations of the effects of interannual and decadal variability on the clear-sky outgoing longwave radiation spectrum. *Q. J. R. Meteorol. Soc.*, **129**, 2971-2988

Brindley, H. and J. Harries, 2003a, The impact of instrument field of view on measurements of cloudy-sky spectral radiances from space: application to IRIS and IMG, *J. Quant. Spect. Rad. Trans.*, **78**, 341-352

Brindley, H. and J. Harries, 2003b, Observations of the infrared outgoing spectrum of the Earth from space: The effects of temporal and spatial sampling, *J. Clim.*, **16**, 3820-3833

Chahine, M., and Coauthors, 2006, AIRS: Improving weather forecasting and providing new data on greenhouse gases. *Bull. Amer. Meteor. Soc.*, **87**, 911-926

Charlock, T., 1984, CO_2 induced climatic-change and spectral variations in the outgoing terrestrial infrared radiation. *Tellus-B*, **36**, 139-148

Charlton, A. and L. Polvani, 2007, A new look at stratospheric sudden warmings. Part 1: Climatology and modeling benchmarks. *J. Clim.*, **20**, 449-469

Goody, R., R. Haskins, W. Abdou and L. Chen, 1995, Detection of climate forcing using emission spectra. *Earth Observation and Remote Sensing*, **13**, 713-722

Griggs, J. and J. Harries, 2007, Comparison of spectrally resolved outgoing longwave radiation over the tropical Pacific between 1970 and 2003 using IRIS, IMG and AIRS. *J. Climate*, **20**, 3982-4001

Hanel, R., B. Conrath, V. Kunde, C. Prabhakara, I. Revah, V. Salomonson and G. Wolford, 1972, The Nimbus 4 infrared spectroscopy experiment,1. Calibrated thermal emission spectra, *J Geophys Res.*, **77**, 2629-2641

Harries, J., H. Brindley, P. Sagoo and R. Bantges, 2001, Increases in greenhouse forcing inferred from the outgoing longwave spectra of the Earth in 1970 and 1997. *Nature*, **410**, 355-357

Harries, J., B. Carli, R. Rizzi, C. Serio, M. Mlynczak, L. Palchetti, T. Maestri, H. Brindley, and G. Masiello, 2008, The Far-infrared Earth, *Rev. Geophys.*, **46**, doi:10.1029/2007RG000233

Hilton, F. and Coauthors, 2012, Hyperspectral Earth observation from IASI: five years of accomplishments. *Bull. Amer. Meteor. Soc*., doi: 10.1175/BAMS-D-11-00027.1

Huang, Y. and V. Ramaswamy, 2008, Observed and simulated seasonal co-variations of outgoing longwave radiation spectrum and surface temperature. *Geophys. Res. Lett*., **35**, doi:10.1029/2008GL034859

Huang, Y. and V. Ramaswamy, 2009, Evolution and Trend of the Outgoing Longwave Radiation Spectrum. *J. Climate*, **22**, 4637-4651

Huang, Y., S. Leroy, P. J. Gero, J. Dykema, and J. Anderson, 2010, Separation of longwave climate feedbacks from spectral observations. *J. Geophys. Res*, **115**, doi:10.1029/2009JD012766

Iacono, M. and S. Clough, 1996, Application of infrared spectrometer clear sky spectral radiance to investigations of climate variability. *J. Geophys., Res*., **101**, 29439-29460

Kato, S., B. Wielicki, F. Rose, X. Liu, P. Taylor, D. Kratz, M. Mlynczak, D. Young, N. Phojanamongkolkii, S. Sun-Mack, W. Miller and Y. Chen, 2011, Detection of atmospheric changes in spatially and temporally averaged infrared spectra observed from space. *J. Clim*., 24, 6392-6407

Kiehl, J., 1986, Changes in the radiative balance of the atmosphere due to increases in CO_2 and trace gases. *Adv. Space Res*., **6**, 55-60

Kirk-Davidoff, D., R. Goody and J. Anderson, 2005, Analysis of sampling errors for climate monitoring satellites. *J. Clim*., **18**, 810-822

Kishore, P., S. Namboothiri, K. Igarashi, J. Jiang, C. Ao and L. Romans, 2006, Climatological characteristics of the tropopause parameters derived from GPS/CHAMP and GPS/SAC-C measurements. *J. Geophys. Res.*, **111**, doi:10.1029/2005JD006827

Larar, A., W. Smith, D. Zhou, H. Revercomb, J. Taylor, S. Newman and P. Schlussel, 2010, IASI spectral radiance validation inter-comparisons: case study assessment from the JAIVEx field campaign. *Atmos. Chem. Phys*., **10**, 411-430

Leroy, S., J. Anderson, J. Dykema, and R. Goody, 2008, Testing climate models using thermal infrared spectra. *J. Climate*, **21,** 1863-1875

Loeb, N., B. Wielicki, D. Doelling, G-L. Smith, D. Keyes, S. Kato, N. Manolo-Smith, T. Wong, 2009, Toward optimal closure of the Earth's Top-of-Atmosphere radiation budget, *J. Climate*, 22, 748-766

Loeb, N., J. Lyman, G. Johnson, R. Allan, D. Doelling, T. Wong, B. Soden, and G. Stephens, 2012, Observed changes in top-of-the-atmosphere radiation and upper-ocean heating consistent within uncertainty. *Nature Geoscience*, **15**, 110-113

Newman, S., F. Hilton, J. Taylor, A. Collard, W. Smith and A. Larar, 2008, Direct radiance validation of IASI-Results from JAIVEx. Tech. Proc. 16th Int. TOVS Study Conf., Angra Dos Reis, Brazil, International TOVS Working Group. [Available online at http://cimss.ssec.wisc.edu/itwg/itsc/itsc16/presentations/-2_08_newman.pdf]

Salby, M., H. Hendon, K. Woodberry and K. Tanaka, Analysis of global cloud imagery from multiple satellites. *Bull. Amer. Meteor. Soc*., , 467-480

Simeoni, D., and 15 co-authors, 2004, Design and development of IASI instrument, Proceedings of SPIE, 5543, 208-219

Sinha, A. and J. Harries, 1995, Water-vapor and greenhouse trapping - the role of far-infrared absorption, *Geophys. Res Lett*., **22**, 2147-2150

Slingo, A. and M. Webb, 1997, The spectral signature of global warming. *Q. J. R. Meteorol. Soc.*, **123**, 293-307

Strabala, K., S. Ackerman and W. Menzel, 1994, Cloud properties inferred from 8-12-mu-m data. *J. Appl. Meteorol*., **33**, 212-229.

Susskind, J., G. Molnar, L. Iredell and N. Loeb, 2012, Interannual variability of outgoing longwave radiation as observed by AIRS and CERES. *J. Geophys. Res.*, **117**, doi: 10.1029/2012JD017997

Wielicki, B. and 39 co-authors, 2013, Achieving climate change accuracy in orbit, *Bull. Amer. Meteor. Soc.*, **94**, 1519-1539

Figure Captions

Figure 1: Average 2008-2012 global, annual mean IRR brightness temperature spectrum. Vertical dashed lines at 700 cm^{-1} and 1303 cm^{-1} are included to help orientate the reader in the discussions concerning spectral features and variability contained in the main text

Figure 2: Standard deviation in 10° zonal, annual mean all-sky IRR brightness temperature spectra for the northern (a) and southern hemisphere (b). Vertical dashed lines are provided at 700 and 1303 cm^{-1}

Figure 3: As Figure 1 for standard deviation in 30° zonal annual mean spectra

Figure 4: (a) Deviation in annual global mean brightness temperature from the five year average global annual mean spectrum shown in Fig 1; (b) Standard deviation in global annual mean IRR brightness temperatures for all 5 years (black) and excluding 2010 (red). Dashed vertical lines as in Figures 1 to 3

Figure 5: (a) Coefficient of Variation (CV) in 10° annual zonal mean window fluxes and radiances measured by CERES and IASI respectively as a function of latitude. (b) Dependence of CV on spatial scale for different spectral regions and instruments

Figure 6: Ratio of window to broadband CV for selected regions for (a) Terra, Aqua and IASI (IRR spectra); (b) IASI as a function of sampling characteristics. (Deep-Tropics: 10°S-10°N; Tropics: 30°S-30°N; NH: 0-90°N; SH 0-90°S; Quasi Global: 60°S-60°N)

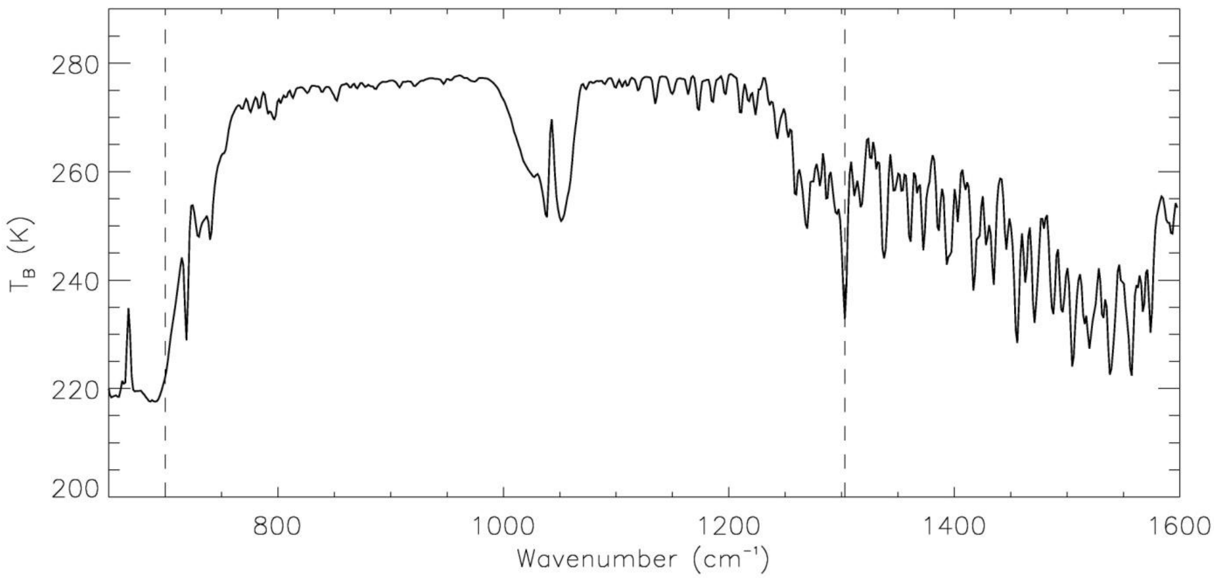

Figure 1: Average 2008-2012 global, annual mean IRR brightness temperature spectrum. Vertical dashed lines at 700 cm^{-1} and 1303 cm^{-1} are included to help orientate the reader in the discussions concerning spectral features and variability contained in the main text.

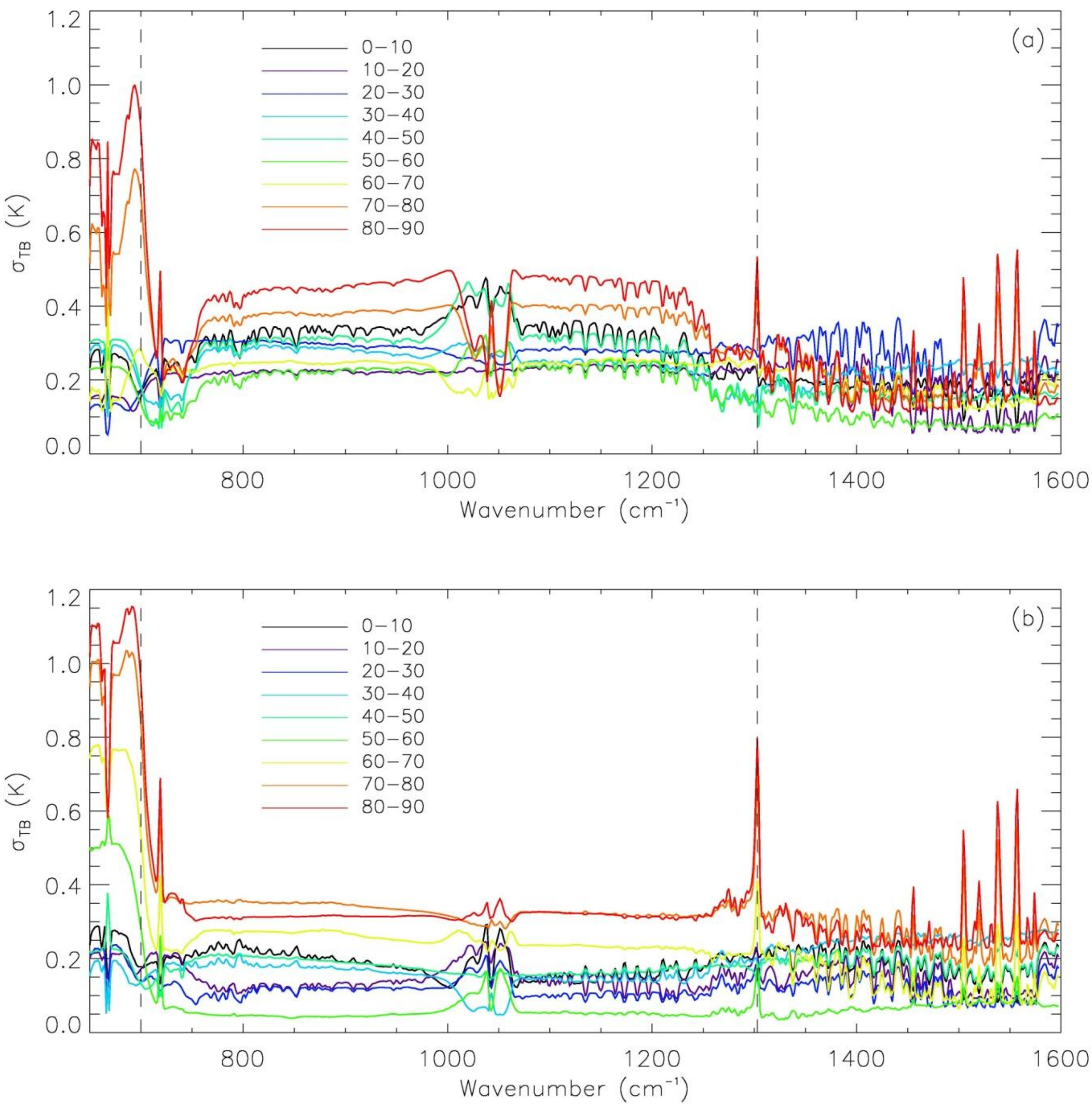

Figure 2: Standard deviation in 10° zonal, annual mean all-sky IRR brightness temperature spectra for the northern (a) and southern hemisphere (b). Vertical dashed lines are provided at 700 and 1303 cm^{-1}

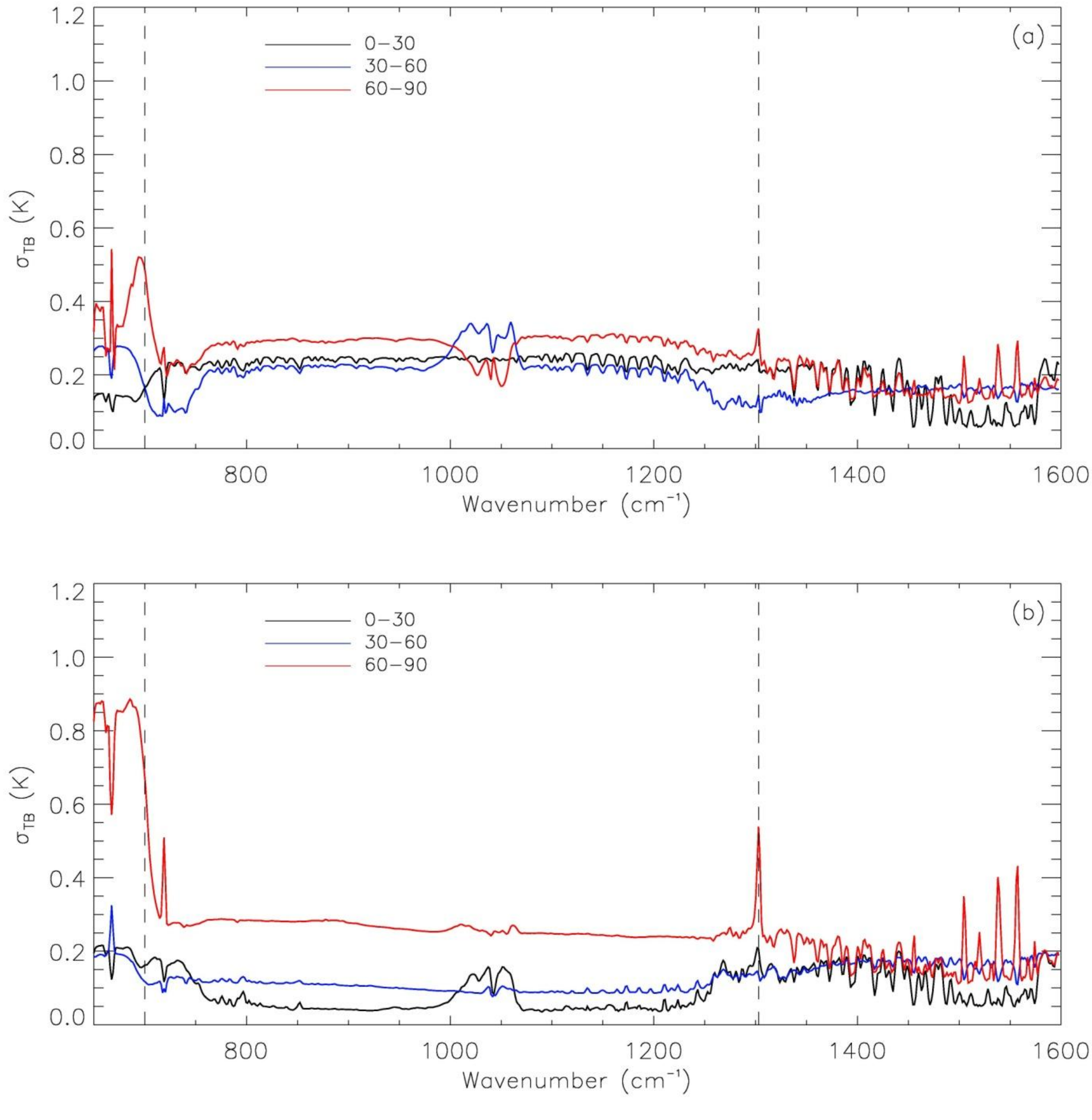

Figure 3: As Figure 1 for standard deviation in 30° zonal annual mean spectra

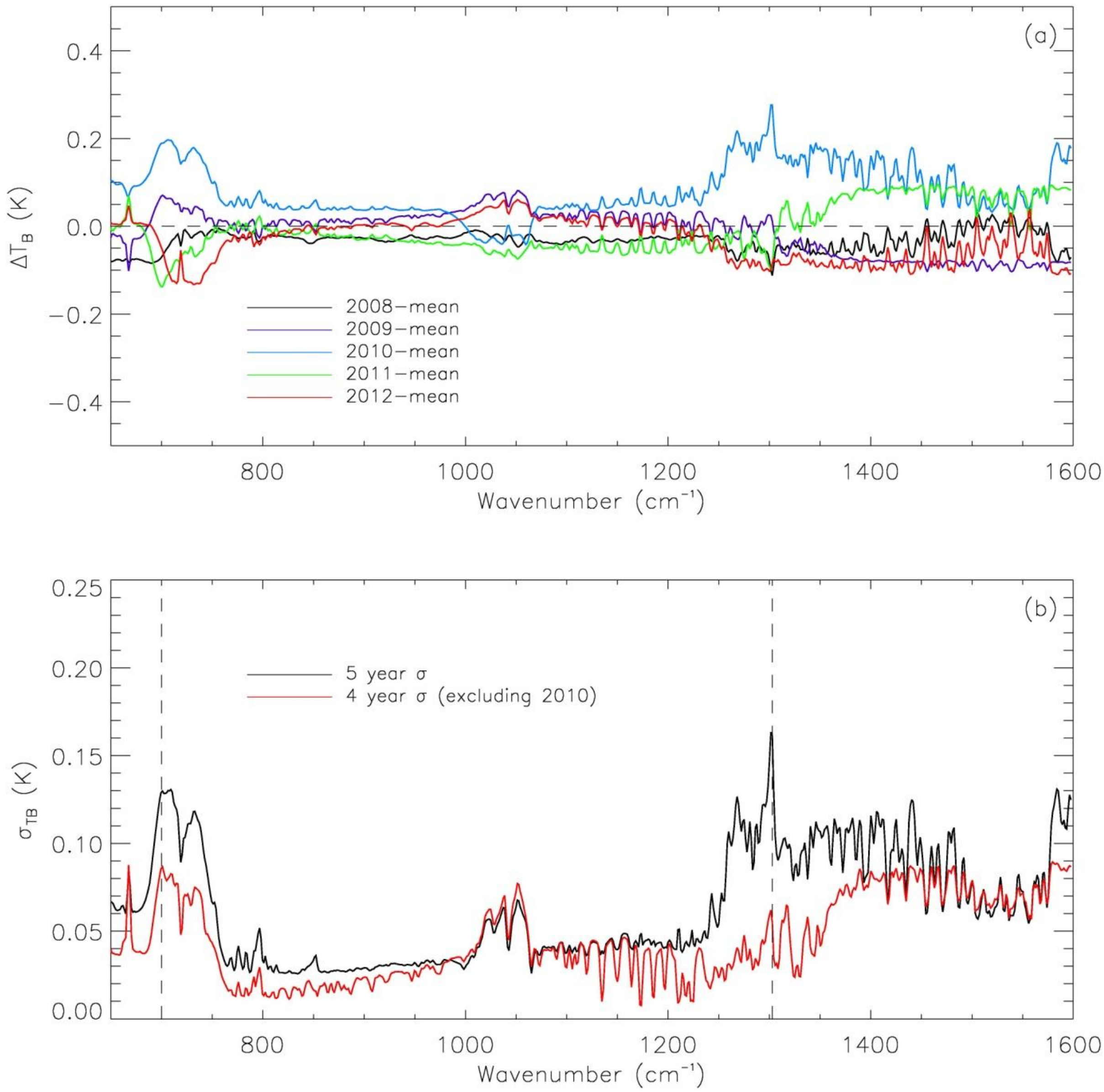

Figure 4: (a) Deviation in annual global mean brightness temperature from the five year average global annual mean spectrum shown in Fig 1; (b) Standard deviation in global annual mean IRR brightness temperatures for all 5 years (black) and excluding 2010 (red). Dashed vertical lines as in Figures 1 to 3

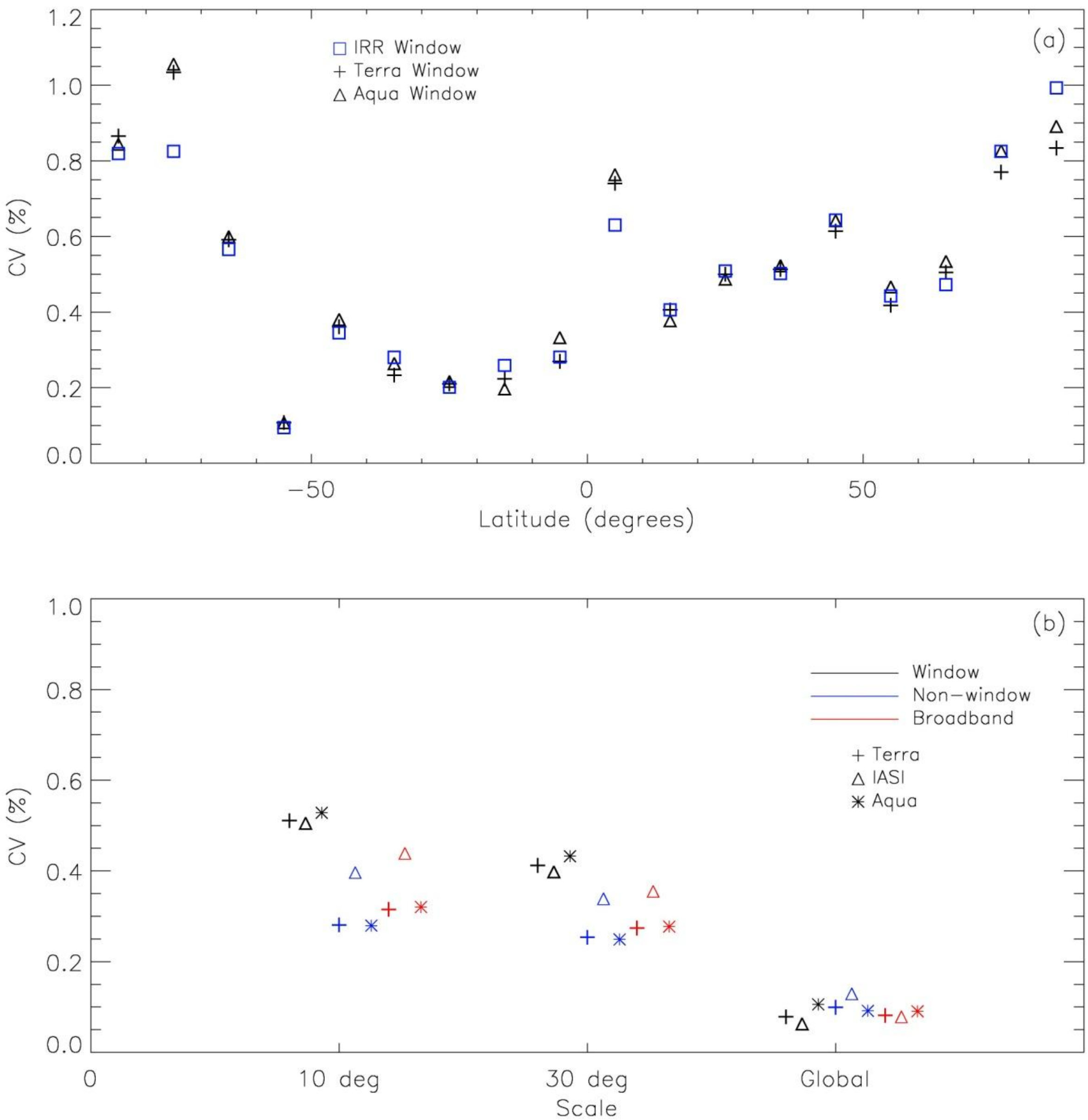

Figure 5: (a) Coefficient of Variation (CV) in 10° annual zonal mean window fluxes and radiances measured by CERES and IASI respectively as a function of latitude. (b) Dependence of CV on spatial scale for different spectral regions and instruments

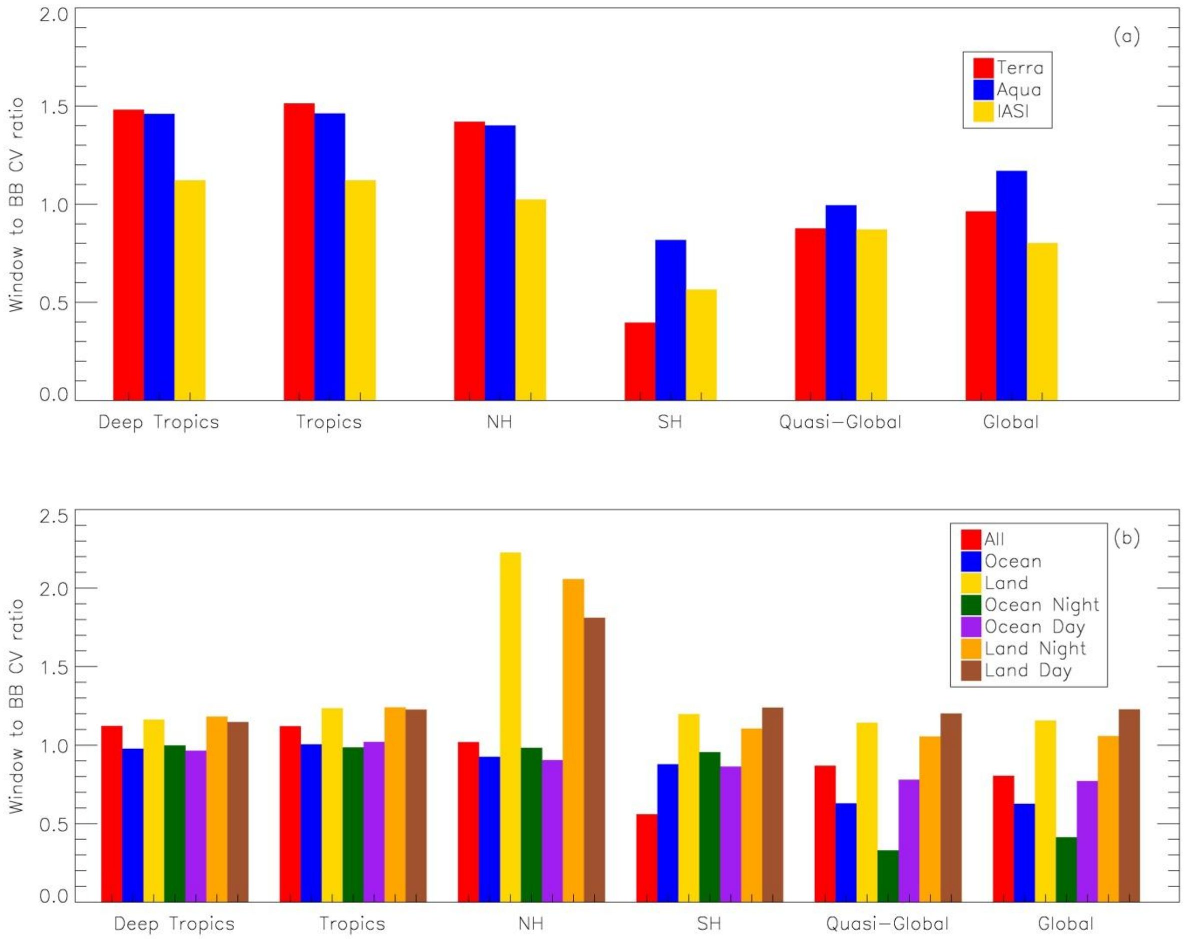

Figure 6: Ratio of window to broadband CV for selected regions for (a) Terra, Aqua and IASI (IRR spectra); (b) IASI as a function of sampling characteristics. (Deep-Tropics: 10°S-10°N; Tropics: 30°S-30°N; NH: 0-90°N; SH 0-90°S; Quasi Global: 60°S-60°N)